Photodisintegration of He^3†*

B. L. Berman, L. J. Koester, Jr., and J. H. Smith
University of Illinois, Urbana, Illinois
(Received 19 August 1963)

The 90° photodisintegration cross sections for He^3 were measured for incident photon energies between 8.5 and 21.5 MeV by detecting proton-deuteron coincidences in CsI(Tl) scintillators immersed in 1 atm of gas. The source of x rays was the bremsstrahlung beam of the University of Illinois 22-MeV betatron. The simultaneous output pulses from the coincidences were displayed on a dual-beam oscilloscope and photographed. The particle energies were determined by pulse-height measurement, and electrons were rejected by pulse-shape analysis. The peak cross section for the $He^3(\gamma,p)d$ reaction, which is very sensitive to the nuclear size, occurs at 10.8±0.3 MeV and equals 0.092±0.004 mb/sr. Gaussian ground-state wave functions for He^3 fail to predict the shape of the cross-section curve. The modified exponential wave function of Gunn and Irving gives a good fit for a root-mean-square nuclear radius of 1.94 F (corresponding to a charge radius of 2.1 F). The He^3 charge form factor calculated with this wave function agrees very well with the electron scattering measurements of Collard and Hofstadter for small momentum transfers q and deviates by 20% only at $q^2=5$ F^{-2}. Also, some information was acquired about the competing three-body photodisintegration process by detecting proton-proton coincidences in the cases where the angle between the two outgoing protons was near either 90 or 180°.

I. INTRODUCTION

As the only stable 3-body nucleus, He^3 is in principle a reasonable starting point for the study of many-body nuclear forces. The understanding of the nature of this nucleus would constitute a major advance towards the solution of the general problem of nuclear forces; in particular, it involves the influence of the third nucleon on the interaction between the other two. This latter interaction has been studied extensively in the deuteron and in nucleon-nucleon scattering. This work is intended as a contribution to the understanding of the structure of the He^3 nucleus and the forces acting therein.

The bombardment of a nucleus with high-energy photons is valuable as a probe of its structure. Electromagnetic reactions give information regarding the charge and magnetic moment distributions inside the nucleus. At energies in the giant resonance region, the electric dipole approximation allows a simple interpretation of the data. Photonuclear reaction theories have been formulated in terms of both the collective and independent-particle models of the nucleus, and integrated photonuclear cross sections are predicted by means of model-insensitive sum rules. Several authors[1–5] have formulated ground-state wave functions of He^3 in terms of the relative coordinates of the nucleons in the nucleus. The validity of such wave functions can be tested by cross-section measurements, and the results related to the nuclear form factors and the root-mean-square radius of He^3.

In this work, the 90° differential cross sections for the photodisintegration of He^3 into a proton and a deuteron have been measured for incident photon energies between 8.5 and 22 MeV. Some information also was acquired on the competing disintegration process into two protons and a neutron. The only previous direct information on these processes was obtained by Cranberg,[6] who measured the energy and angular distribution of the charged reaction products in nuclear emulsions.

The inverse reaction, $p+d\rightarrow He^3+\gamma$, has been studied by several investigators.[7–11] The results of these experiments can be summarized as follows: (a) There is a single γ ray of energy approximately equal to $\frac{2}{3}E_p+5.49$ MeV, where E_p is the incident proton energy; (b) The angular distribution of the γ rays is $b+\sin^2\theta$, where b is small; this, together with polarization measurements, indicates that the dominant reaction process is direct radiative capture of p-wave protons to the final ^2S ground state of He^3, for which the emitted radiation is electric dipole. This cross section can be related to that for 2-body photodisintegration of He^3 by a detailed balance calculation.

The present experiment was done with the bremsstrahlung beam of a 22-MeV betatron incident upon a He^3 gas target. Coincidences were demanded between

† This work supported in part by the U. S. Office of Naval Research.
* A preliminary account of this work appeared as B. L. Berman, L. J. Koester, Jr., and J. H. Smith, Phys. Rev. Letters **10**, 527 (1963).
[1] M. Verde, Helv. Phys. Acta **23**, 453 (1950).
[2] J. C. Gunn and J. Irving, Phil. Mag. **42**, 1353 (1951).
[3] C. Rossetti, Nuovo Cimento **14**, 1171 (1959).
[4] T. Kikuta, M. Morita, and M. Yamada, Progr. Theoret. Phys. (Kyoto) **15**, 222 (1956).
[5] J. N. Pappademos, Nucl. Phys. **42**, 122 (1963).
[6] L. Cranberg, Bull. Am. Phys. Soc. **3**, 173 (1958), and private communication. Thanks are due to Dr. Cranberg for communicating his unpublished results.
[7] S. C. Curran and J. Strothers, Proc. Roy. Soc. (London) **172**, 72 (1939).
[8] W. A. Fowler, C. C. Lauritsen, and A. V. Tollestrup, Phys. Rev. **76**, 1767 (1949).
[9] D. H. Wilkinson, Phil. Mag. **43**, 659 (1952).
[10] G. M. Griffiths and J. B. Warren, Proc. Phys. Soc. (London) **68**, 781 (1955).
[11] G. M. Griffiths, E. A. Larson, and L. P. Robertson, Can. J. Phys. **40**, 402 (1962).

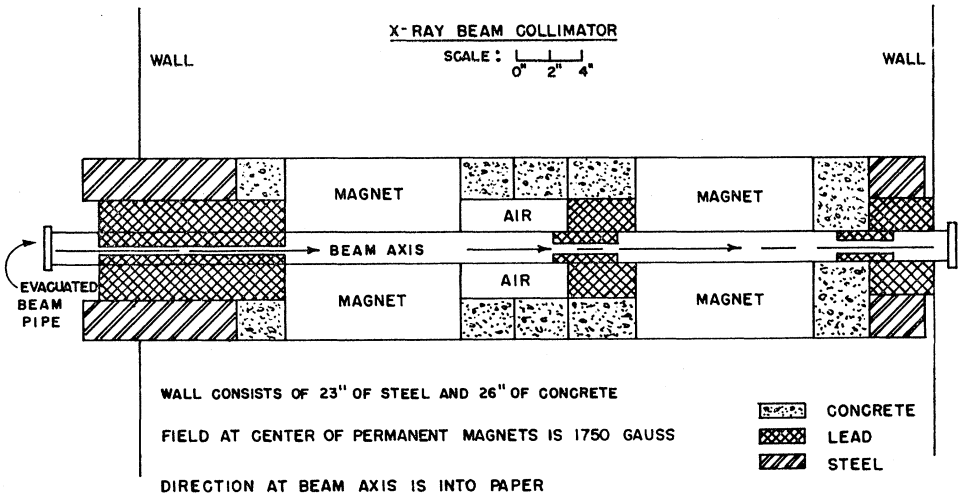

FIG. 1. Cut-away view of the x-ray beam collimator and shielding wall.

the proton and the deuteron from the 2-body disintegrations, with CsI(Tl) scintillators as detectors. The particle energies were determined by pulse-height measurement, and electrons were rejected by pulse-shape analysis. Because the incident photon momentum is small at energies up to 22 MeV, the proton and deuteron are emitted nearly back-to-back in the laboratory system, with nearly equal momenta. Hence, the energy of the proton is about twice that of the deuteron, which constitutes a unique signature for this process. In the competing 3-body disintegrations, the angular correlation and relative energy of the two protons are not similarly fixed by kinematics.

II. APPARATUS AND EXPERIMENTAL PROCEDURE

The betatron energy calibration was checked by measuring the activity induced in irradiated Cu^{63} and C^{12} samples as a function of betatron energy near the photoneutron thresholds for these materials. During the experiment, the betatron energy was held constant to $\pm 0.1\%$ at 22 MeV by a magnet amplitude regulator. The x-ray beam was extracted with a 300-μsec duration 180 times/sec.

Three lead collimators were set inside an evacuated beam pipe which in turn passed through a 49-in. steel and concrete shielding wall (Fig. 1). The entrance hole of the primary collimator was $\frac{1}{4}$ in. square and was positioned 34.25 in. from the electron target. Permanent magnets between the collimators swept electrons and positrons out of the beam (Fig. 1). Thus, a clean beam, 2 cm square and diverging with a $\frac{1}{4}°$ half-angle, was obtained at the position of the He^3 target chamber, 66.75 in. from the primary collimator.

The incident flux was measured by an NBS-type[12] Dural ionization chamber and vibrating reed electrometer located 22 ft. beyond the target chamber. The electrometer response was measured three times during the course of the experiment and did not change. The beam size at the position of the monitor was 3 in. Monitor drift was neglected on the basis of repeated tests which showed it to be small and random.

The He^3 gas was stored in a stainless steel tank after passing through a liquid-helium trap for removal of contaminants. It was transferred by means of a glass Toepler pump, and passed through a liquid-nitrogen trap just before entering the target chamber.

The target chamber (Fig. 2) was constructed of brass, with thin Alumiseal windows for the x-ray beam. Alumiseal, a Mylar-aluminum laminate, served both as a light seal and as a thin barrier through which the diffusion rate of helium is extremely small. The chamber was filled with He^3 gas at slightly less than atmospheric pressure, so that the chamber was a constant-volume device of 0.5 liter capacity. The average density of He^3 in the chamber during the experimental runs was 0.855 ± 0.008 times the density of He^3 at 15°C and 760 mm Hg.

CsI(Tl) crystals, 2.83 cm square and 1 mm thick, were mounted symmetrically inside the chamber 5 cm

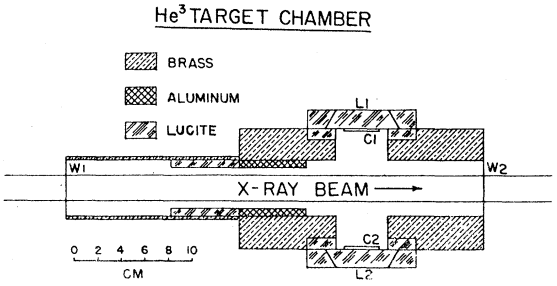

FIG. 2. He^3 target chamber. $C1$ and $C2$ are CsI(Tl) crystals, $L1$ and $L2$ are light pipes, and $W1$ and $W2$ are thin Alumiseal windows. Gaskets and flanges are omitted for clarity.

[12] J. S. Pruitt and S. R. Domen, National Bureau of Standards Report No. 6218, 1958 (unpublished).

from the beam axis (Fig. 2). These crystals were thick enough to stop any of the heavy charged particles produced. A second pair of identical counters (not shown in the figure) was mounted at right angles to the first, in order to double the effective counting rate, to detect 3-body disintegrations when the two protons are emitted at 90° to each other, and to make use of the anisotropic distribution of cosmic rays for tests and background calibration. To reduce the electron background at the crystals from pair production and Compton scattering in the entrance window, aluminum and Lucite baffles with square holes were inserted along the beam in the chamber as shown, and the entrance window itself was placed far from the crystals. The conical Lucite light pipes also served as gas-tight windows, and were silvered on all surfaces except where they were in contact with the crystals and phototubes. An evaporated layer of aluminum about 0.5 mg/cm² thick on the surface of each crystal completed the reflecting enclosure. The silvered and aluminized surfaces were held at high voltage so that there would be no large stray electrostatic fields in the neighborhood of the photocathodes, and were insulated from the body of the chamber with Lucite rings (Fig. 2). The entire target chamber was aligned telescopically and by means of x-ray photographs along the collimator axis. Uncertainties in alignment and positioning were calculated to cause errors of less than 1%.

The RCA-6655A photomultiplier tubes were run at about 1100 V, with the anodes grounded. The high voltages were checked frequently with a Rawson electrostatic voltmeter and found to be constant to ±0.3%. The singles rate in any one of the counters was so low that the probability of two particles arriving within 10 μsec was very small. This fact, together with the low-duty cycle of the betatron, assured that the photocathodes would not be fatigued. The signals for the pulse-height measurement were taken from the last dynodes and displayed on a Tektronix 551 dual-beam oscilloscope which was triggered by coincidences taken from the anodes. These dynode signals were integrated with an RC time constant of 1 μsec, comparable to the fluorescent decay time constants of CsI(Tl), at the inputs of transistorized high-impedance linear preamplifiers (Ckt. D, Fig. 3) having a gain of about 0.7. The preamplifiers were tested with a mercury switch pulser and found to be linear to ±2%, until saturating hard for input pulses of 4.8 V. The dynode pulses in the experimental runs ranged from 0.4 to 4.3 V. The preamplifier outputs were displayed on the oscilloscope. A signal from one counter of each pair was displayed on the upper trace. The positions of the pulses on the trace designated with which pair of counters the event was detected. An example is shown in Fig. 4.

The logic signals from the anodes were fed into similar preamplifiers as shown (Ckt. A, Fig. 3). A block diagram of the logic circuitry is shown in Fig. 5. The differentiated "fast" anode outputs operated fast coincidence circuits with trigger discriminator inputs. The trigger widths were 67 nsec, and the discriminators were set so that the 1-MeV deuterons would produce a trigger pulse. A partially integrated (rise time 0.4 μsec) "slow" anode signal, at least as large as those caused by 2-MeV protons, was required to produce a second trigger pulse, thus discriminating against many events, particularly those involving electrons or γ rays, which could not be 2-body disintegrations of He^3. These trigger widths were 2 μsec. A coincidence was demanded between the output of one of the fast coincidence circuits, suitably delayed to compensate for the integration time of the slow anodes, and that of one of the slow anode triggers. This was accomplished with the use of OR circuits as shown in Fig. 5. The output of this slow coincidence circuit then triggered the oscilloscope, and both it and the oscilloscope were monitored with scalers. The gate output of the oscilloscope was used to advance the camera which photographed the integrated dynode signals. The fast triggers were gated on for 700 μsec by the expander trigger of the betatron, and both this gate signal and the x-ray pulse shape were monitored continuously on a Tektronix 543 oscilloscope (Fig. 5).

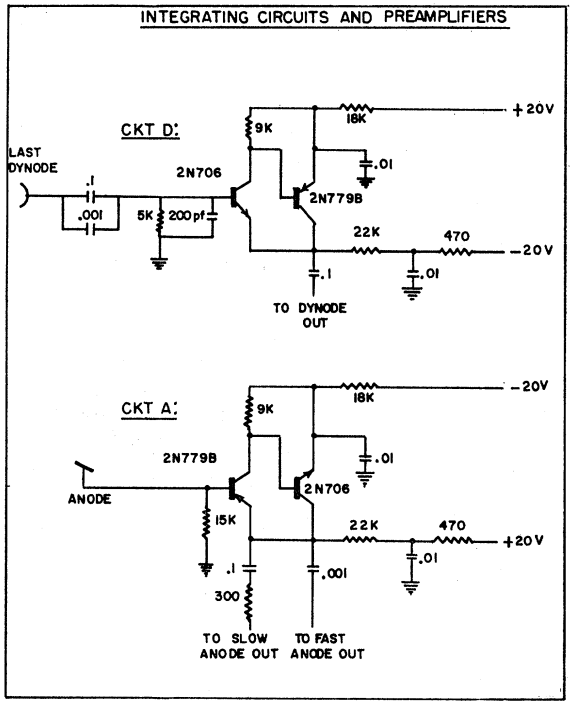

FIG. 3. Circuit diagrams of the integrating circuits and preamplifiers.

The modular logic circuits used were developed in the electronics laboratory of the high-energy physics group at the University of Illinois. The testing procedure consisted of: (a) calibrating the oscilloscope amplifiers with internally generated square-wave signals; (b) setting the phototube voltages with peak pulses from

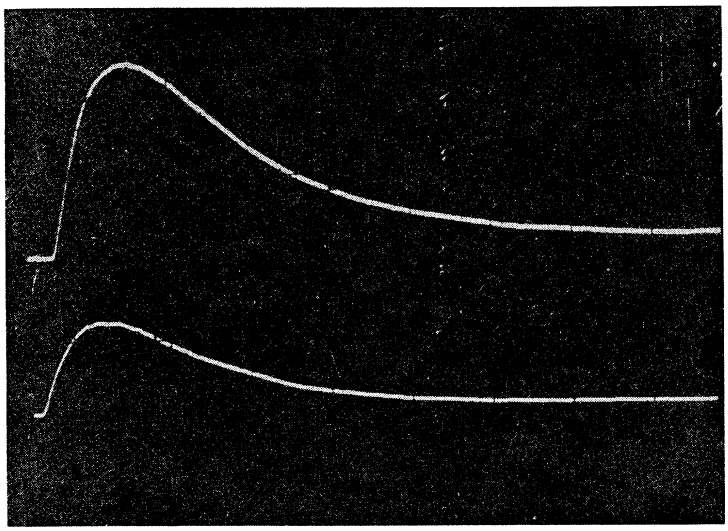

FIG. 4. Oscilloscope photograph of a typical $He^3(\gamma,p)d$ event.

Cs^{137} and Co^{60} sources and from photodisintegration of deuterium and He^3; (c) calibrating the trigger discriminator levels with a mercury switch pulser; (d) making sure the fast anode triggers fired on sufficiently large events; and (e) setting the slow, and then the fast anode trigger discriminator levels.

The main experiment consisted of two parts. One set of experimental runs was taken at fairly high discriminator level settings on the slow anode triggers (but low enough to permit 2-MeV protons to fire them), with the x-ray beam intensity about half the maximum available. These runs were displayed at 1 V/cm deflection sensitivity on the dual-beam oscilloscope. A sweep speed of 1 μsec/cm was used throughout the experiment. The highest energy protons produced oscilloscope deflections of about 3.4 cm on these runs. The other set of runs was taken at much lower discriminator settings, allowing a large safety factor to make sure that no losses were suffered for the lowest energy events. These were displayed on the 0.5 V/cm scales of the oscilloscope to double the reading sensitivity. On these runs, the beam intensity had to be reduced by about one-third in order to keep the camera advancing at the same rate as for the 1 V/cm runs, averaging about 1 event every 5 sec. Most events were caused by electrons or γ rays, and were small: on the 1 V/cm runs, about 1 event in 6 represented a He^3 disintegration; on the 0.5 V/cm runs, about 1 in 12.

In addition, a number of runs were taken without demanding coincidences between the counters. These singles runs were taken primarily as a check on the gain calibrations of the four channels, with both 16 and 22 MeV bremsstrahlung beams. Also, several runs demanding coincidences between pairs of counters located at right angles to each other were taken at 22 MeV. Events of this nature necessarily must be 3-body disintegrations, and hence give information on this process without interference from the much higher counting rates of the 2-body disintegrations. Finally, a number of background tests were performed: cosmic-ray coincidences and betatron runs with He^4 gas in the target chamber, both at normal and reduced pressures; runs with the counters intentionally out of coincidence, which showed the accidental rate to be negligible and to result from electrons; and a run taken with $\frac{5}{8}$-in. circular apertures placed in front of two of the CsI(Tl) crystals.

The photographs were taken on 35 mm Kodak Tri-X film with a Bell and Howell Model D animation camera,

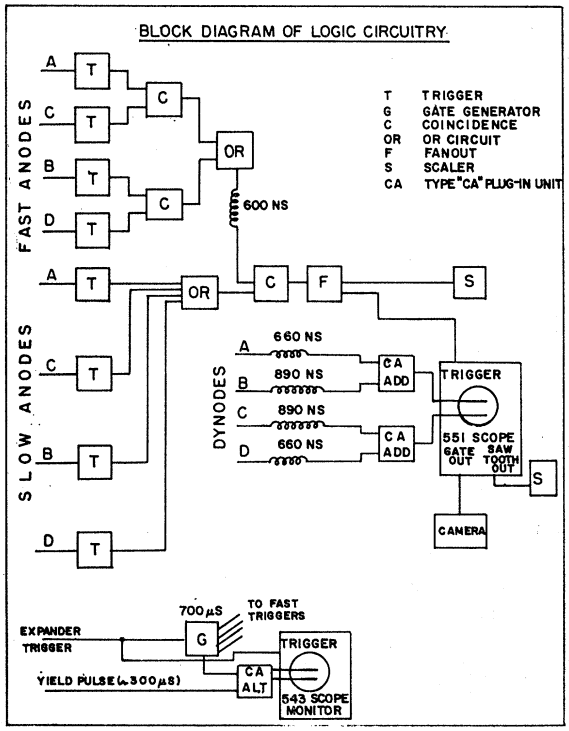

FIG. 5. Block diagram of the logic circuitry.

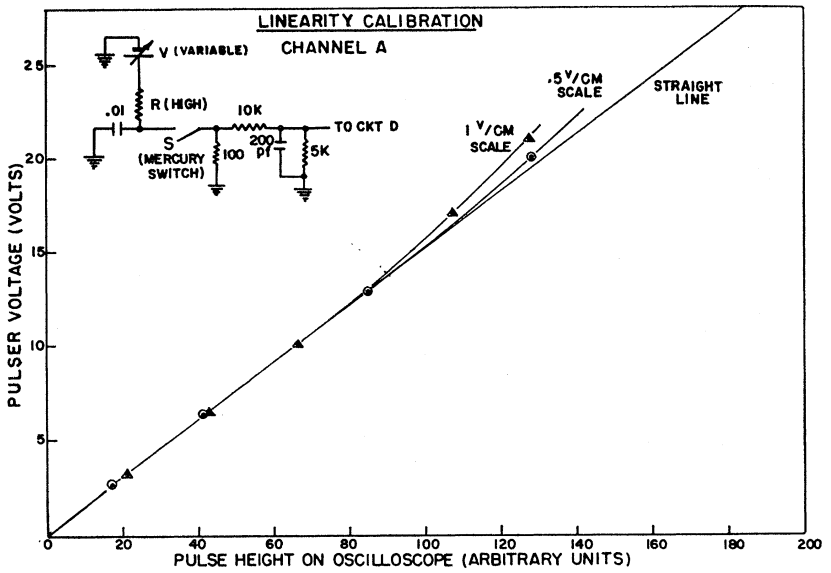

FIG. 6. Circuit diagram and pulse-height plot for the linearity calibration of the preamplifiers and oscilloscope.

capable of repeat operation in 0.4 sec. The developed film could be repositioned and projected accurately with a similar camera. The dc levels of the scope traces were fixed by batteries to prevent drift. A magnification of 4.16 was used, and the reading errors ranged from about $\pm 0.5\%$ for the largest signals to $\pm 5\%$ for the smallest. Distortion owing to the optical system was measured to be less than 0.5%.

The linearity calibration of the preamplifiers and oscilloscope was accomplished by simulating typical phototube signals with a mercury switch pulser and RC network and feeding them directly into the dynode channels (Fig. 6). Film was exposed, developed, and projected in the usual way, and the nonlinearity of each channel was determined for both the 1 and 0.5 V/cm scales. Corrections to the pulse-height readings were zero for most events, were less than 5% for nearly all the events corrected, and never exceeded 12% (Fig. 6).

The pulse-shape analysis consisted of comparing the pulse amplitude at 3.6 μsec (15 cm after the beginning of the pulse as projected) with the peak height. This procedure takes advantage of the variation of the

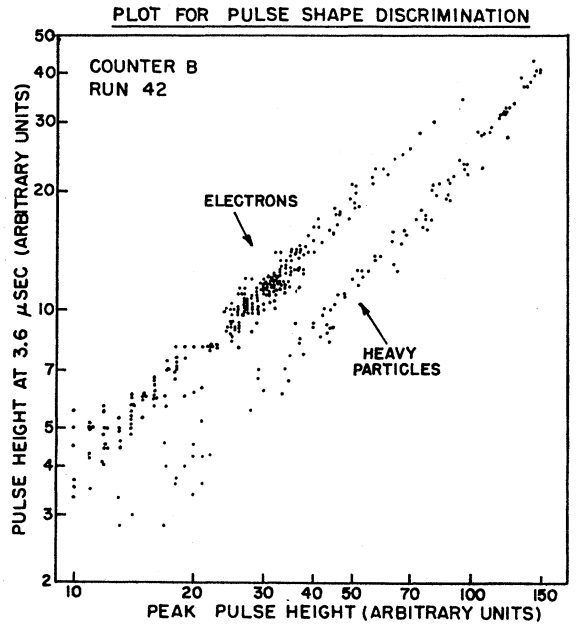

FIG. 7. Plot of peak pulse height versus pulse height at a later time for distinguishing heavy-particle events from those caused by electrons or γ rays.

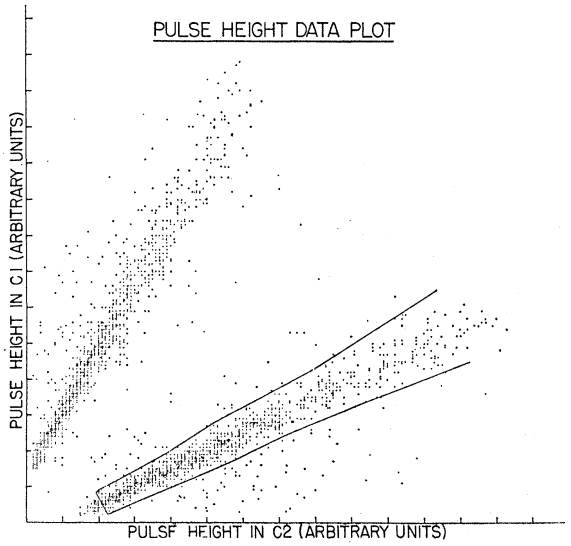

FIG. 8. Data points from counters *C*1 and *C*2. Points in the densely populated areas are p-d coincidences from $He^3(\gamma,p)d$. The solid lines are drawn on the lower branch to show our boundaries for excluding scattered p-p coincidences from $He^3(\gamma,2p)n$ (see text) and the cutoff at 8.5 MeV incident photon energy.

fluorescent decay time constant of CsI(Tl) with ionization density, and hence, with particle velocity.[13,14] Electrons in this energy range, being relativistic, have a longer time constant than the slower heavy particles[13]; this leads to a striking separation of the two groups of events when plotted on log paper (Fig. 7), and makes identification clear.

A breakdown of the 51 232 photographs analyzed appears in Table I.

The number of events detected by each pair of counters was the same, within statistical fluctuations. After the data were corrected for nonlinearities in the preamplifiers and oscilloscope, they were displayed by plotting the peak height in one counter versus the peak height in the opposite counter. Some 2000 events appear in Fig. 8, where the clustering of points around the two-to-one pulse-height ratio characteristic of 2-body disintegration is readily apparent.

TABLE I. Breakdown of analyzed photographs.

Oscilloscope deflection sensitivity	Total number of events	Pairs of heavy particles	Total amount of beam energy
1 V/cm	26 120	4432	8.820 joules
0.5 V/cm	25 112	2125[a]	5.782 joules

[a] Not including events which caused off-scale deflections.

III. DATA ANALYSIS AND RESULTS

The kinetic energy T_p of the proton emitted in a 2-body disintegration is related to its angle of emission by

$$T_p=\frac{1}{2M_p}\left[\frac{k\cos\theta_p+(k^2\cos^2\theta_p+[1+(M_d/M_p)][-k^2+2M_d(k-\delta)])^{1/2}}{1+(M_d/M_p)}\right]^2 \quad (1)$$

or

$$T_p\cong(k\cos\theta_p+[k^2\cos^2\theta_p-3k^2+12M(k-\delta)]^{1/2})^2/18M\,, \quad (2)$$

where M_p and M_d are the masses of the proton and deuteron, respectively, k is the photon energy, $\delta=5.493$ MeV is the threshold energy for the reaction, θ_p is the angle the outgoing proton makes with the incident photon direction in the laboratory system, and $M=\frac{1}{2}[M_p+(M_d/2)]$. The kinetic energy T_d of the deuteron is given by energy conservation. For the case where the two particles are emitted perpendicular to the photon direction in the center-of-mass system,

$$T_p\cong\frac{2(k-\delta)}{3}-\frac{k^2}{18M} \quad (3)$$

and

$$T_d\cong\frac{k-\delta}{3}+\frac{k^2}{18M}\,. \quad (4)$$

Units where $c=1$ have been used throughout.

The spread in the p-d points (Fig. 8) is caused by: (a) the kinematical spread associated with the finite beam width and the angular interval subtended by the counters; (b) the spread in energy loss of the charged particles owing to the varying path lengths of gas traversed; (c) the instrumental resolution. The extreme distances traveled in the gas are the equivalent of 3.64 and 5.25 cm at 15°C and 760 mm Hg. The energy losses of the protons and deuterons in the He^3 gas were calculated as a function of the energy of the incident photon for the extreme and average cases. To these were added the energy losses sustained by the charged particles in traversing the aluminum crystal coating. Finally, the light output of the CsI(Tl) crystals was corrected for the variation in scintillator efficiency with the specific ionization of the incident charged particle.[15,16] The results are summarized in Fig. 9.

To determine the relative gains of the four counters a center-of-gravity method was used. First, those points far from the p-d locus, i.e., far from the region of dense clustering of points on Fig. 8, were excluded from consideration. Then, for each counter, the sum of the proton pulse heights from all the 1 V/cm runs was calculated for all pulses greater than the reading cutoff. This sum was divided by the number of events contributing to it to give the center of gravity of these pulse heights for each counter, which in turn gave a first approximation to the relative gains of the counters. On the basis of these approximate relative gains, the lower limit was then raised appropriately for all but the counter having the lowest gain, and the process was repeated to obtain a better approximation to the true relative gains. This iteration procedure, which converges rapidly, was carried out until no further changes occurred and gave the relative gains to about 1.0%.

The aboslute gains of the counters were determined by fitting the data to the high-energy cutoff of the bremsstrahlung spectrum. First, all pulse heights were referred to a single counter by means of the relative gains. Then the sums of the proton and deuteron pulse heights for each event were grouped into bins, and the number of events was plotted against this sum of pulse

[13] R. S. Storey, W. Jack, and A. Ward, Proc. Phys. Soc. (London) 72, 1 (1958).
[14] J. C. Robertson and J. G. Lynch, Proc. Phys. Soc. (London) 77, 751 (1961).
[15] R. Gwin and R. B. Murray, AEC Report ORNL-3354, 1962 (unpublished), and Phys. Rev. 131, 501 (1963).
[16] R. B. Murray and A. Meyer, Phys. Rev. 122, 815 (1961).

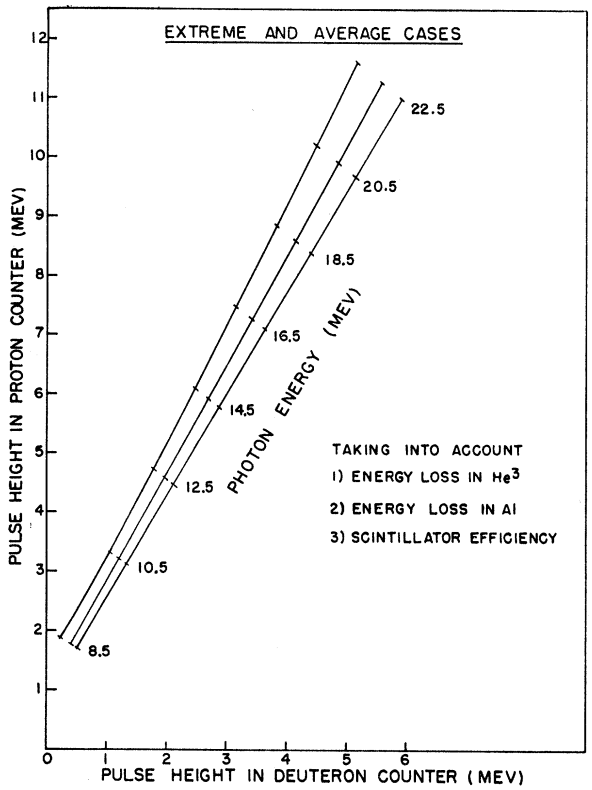

FIG. 9. Kinematical curves for the extreme cases allowed by geometry and the 90° in the center-of-mass case, taking into account energy losses and scintillator efficiency.

heights. These points were compared with the family of theoretical curves obtained for different values of the counter gain. These curves represented the product of the bremsstrahlung cross section[17] and a "typical" 2-body photodisintegration cross section for He^3, suitably normalized. In the actual case, the Verde[1] cross section was used, although any cross section which is slowly varying in the neighborhood of 22 MeV would have done as well, since it is the rapidly varying bremsstrahlung cross section that effectively determines the shape of the yield curve near its high-energy cutoff, and the absolute cross-section value does not enter into this analysis. The results are shown graphically in Fig. 10. Absolute gains were thus determined with an accuracy of 1%. Several checks of the relative and absolute gains of the counters have been made, all of which have been found to be in agreement with the values chosen by the method above, although none is so precise.

After the absolute gains were obtained in this way, the extreme and average curves of Fig. 9 were calculated for each channel and compared with the data plots, e.g., Fig. 8. As expected, the average curves lay astride the most densely populated parts of the *p-d* loci, and the extreme curves contained about 85% of the accepted events. The limits actually used were chosen to coincide with the abrupt change in density of the data points (Fig. 8) instead of the calculated extremes, on the reasonable assumption that the instrumental resolution accounts for the additional spread necessary to extend the limits this far. The error in either direction introduced by this procedure is compensated to a high degree by the method of subtraction of the background of *p-p* coincidences from the 3-body disintegration.

With the aid of the points calculated for the extreme and average curves, lines of constant photon energy (isochromats) were drawn for the 2-body disintegrations. These, together with the limits chosen above, formed bins with a width of 1 MeV in photon energy (Fig. 11). The number of events falling into each bin for each of the four *p-d* loci was counted. The 0.5 V/cm data were treated in the same way as the 1 V/cm data, except that the photon energies involved were 8.5 to 14.5 MeV rather than 8.5 to 22 MeV (events due to higher energy photons produced dynode signals that caused off-scale oscilloscope deflections), and that the corrections for nonlinearities in the amplifiers were only about half as large.

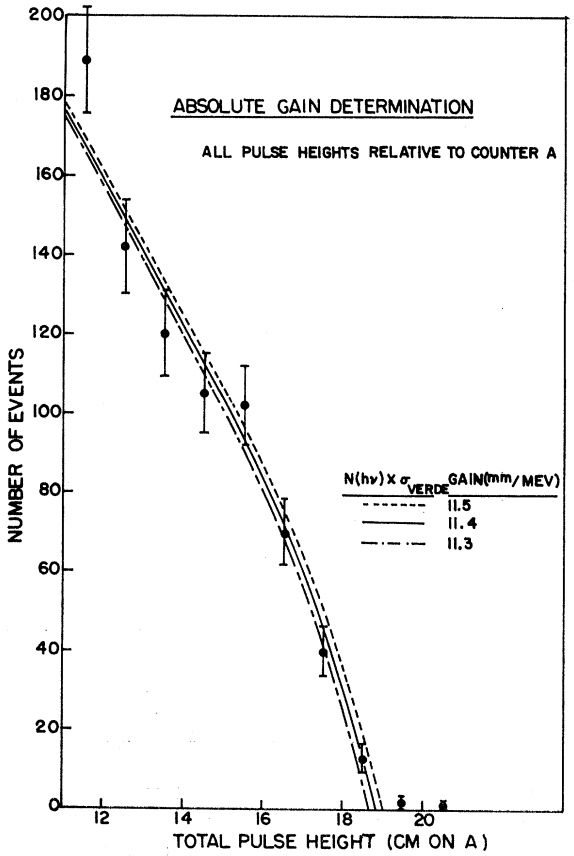

FIG. 10. Fitting of the events with the largest total pulse height to the high-energy cutoff of the bremsstrahlung spectrum to determine the absolute gains of the counters.

[17] A. S. Penfold and J. E. Leiss, Phys. Res. Lab., University of Illinois, 1958 (unpublished).

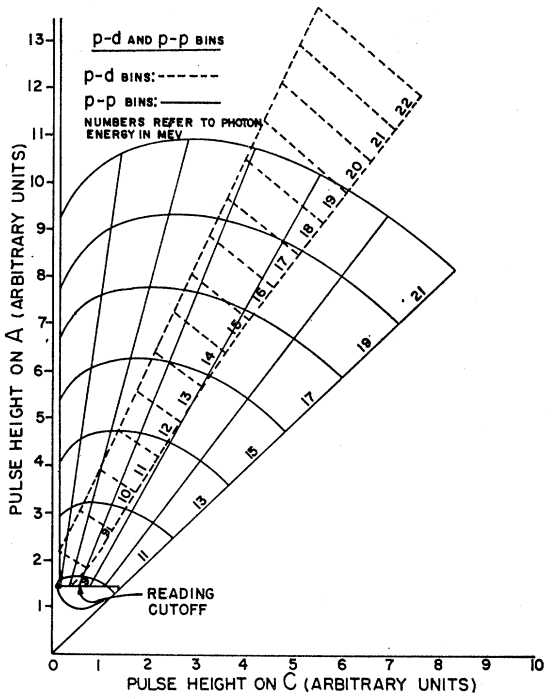

FIG. 11. Plot of the p-d and p-p bins according to photon energy.

The background of p-p coincidences from 3-body disintegrations must be subtracted in some way to account for the p-p's which overlap the p-d loci. For 3-body photodisintegration, neglecting the momentum of the incident photon,

$$T_1+T_2+(T_1T_2)^{1/2}\cos\theta=(k-\delta')/2, \qquad (5)$$

where T_1 and T_2 are the kinetic energies of the two outgoing protons, θ is the angle between them, and $\delta'=7.72$ MeV is the threshold energy for this process. Assuming that all the p-p events in this experiment occur for $\theta=180°$, the isochromats for the 3-body process become the family of ellipses in the (T_1,T_2) plane given by Eq. (5) with $\cos\theta=-1$ for various photon energies k. The (T_1,T_2) plane was divided into bins with a width of 2 MeV in photon energy (with elliptical boundaries) and into bins representing an interval of T_1/T_2 (with boundaries consisting of straight lines passing through the origin) as in Fig. 11. The boundaries were corrected for the variation in the gains of the four channels, and the number of events in each bin or the part of each bin outside the p-d loci was counted. The areas of all bins were measured graphically. Errors other than statistical ones were considered negligible.

The densities of p-p events were plotted as functions $D_1(k)$ and $D_2(T_1/T_2)$. In view of the small numbers of events, the assumption was made that the density variation was smooth and that the density at any point on Fig. 11 could be represented by the normalized product $D_1(k)D_2(T_1/T_2)$. Densities thus obtained for the centers of the p-d bins were multiplied by the measured areas of these bins, and the resulting numbers of events were subtracted from the total number of events in each bin. This method automatically compensates for errors in either direction in defining the limits of the p-d bins, since in the region of these limits, the densities of p-p and p-d points are comparable, and the areas of the bins involved will vary in such a way as to keep the corrected number of p-d events in each bin very nearly constant.

There are 5635 events which satisfy the criteria for 2-body disintegration with incident photon energy above 8.5 MeV, and 584 events which are considered to be p-p coincidences. The number of events subtracted from each p-d bin to account for the p-p background varies from zero (at $k\geq 20$ MeV) to 9.0% (at $k=14$ MeV), and averages 6.0%. The estimated errors in these corrections range from $\pm 20\%$ for high photon energies to $\pm 30\%$ for low energies.

Two further contributions to the p-p background were calculated to be small: (a) p-d coincidences where one of the particles scatters off the brass wall of the chamber into the CsI(Tl) crystal contribute at most 4%, and probably less than 1% of the "p-p" events; (b) p-n coincidences where the neutron causes a nuclear reaction in the CsI(Tl) emitting a charged particle which then looks like a p-d or p-p event contribute less than 0.1%.

The absolute cross section for 2-body photodisintegration is obtained from the expression for the yield (the number of events in each bin) Y:

$$Y=FN\bar{\Omega}\frac{d\sigma}{d\Omega}, \qquad (6)$$

where F is the incident flux, i.e., the number of photons per unit cross-sectional area of the incident x-ray beam in the energy interval corresponding to this bin, N is the number of target nuclei in the interaction volume, $\bar{\Omega}$ is the effective solid angle, and $d\sigma/d\Omega$ is the differential cross section.

The flux of photons $F(h\nu)$ in a bin of width Δ centered at energy $h\nu$ for a bremstsrahlung spectrum having a high-energy limit χ is

$$F(h\nu)=\frac{W}{A}\cdot\int_{h\nu-(\Delta/2)}^{h\nu+(\Delta/2)}(\Phi/k)dk\Big/\int_0^{\chi}\Phi dk, \qquad (7)$$

where A is the cross-sectional area of the beam, and where $\Phi=\Phi(k,\chi)$ is a dimensionless function proportional to k times the bremsstrahlung cross section. The value for $\int_0^{\chi}\Phi dk$ for $\chi=22$ MeV is given by Penfold and Leiss[17] to be 8.625 MeV, and the integral in the numerator of Eq. (7) was found graphically from values of $\Phi(k, 22\text{ MeV})$ given in the same reference for $\Delta=1$

MeV. The energy W in the beam was measured with the beam monitor (see Sec. II).

The solid angle Ω was calculated for 175 equally spaced points spanning one octant of the interaction volume under the assumption that the two outgoing particles were emitted back-to-back in the laboratory system. This is a very good approximation since the angle between the outgoing proton and deuteron is very nearly constant for all possible cases ($172°\pm1°$); the result is that the interaction volume is unchanged in size but merely is displaced slightly. The resulting error in solid angle does not exceed 1.0%. The x-ray beam intensity did not vary appreciably over the cross-sectional area of the beam; hence, the 175 points were given equal weight when added together. The sum was divided by 175 and multiplied by the volume of the octant and the atomic density of the gas to determine $N\bar{\Omega}$ for each of the four counters.

The yield Y is obtained by correcting the number of points $N(p\text{-}d)$ in each bin for: (a) those events which were spoiled because they occurred while the camera was advancing; and (b) those events which could not be read unambiguously because two or more appeared on the same frame. These two effects together constitute $(13.18\pm0.05)\%$ of the events for the 1 V/cm runs and $(13.15\pm0.05)\%$ for the 0.5 V/cm runs, and the number of analyzed events is modified accordingly to get Y. Also, Y is divided by 4, the number of counters. The values of $d\sigma/d\Omega$ are given in Table II. The errors are compounded mostly from the statistical error, but include the estimated error in the correction for $p\text{-}p$ events added quadratically to the statistical error. The cross section is plotted in Fig. 12.

TABLE II. Two-body cross section data.

k(MeV)	$\left.\frac{d\sigma}{d\Omega}\right\|_{90°}$ (mb/sr)
9	0.0800±0.0029
10	0.0908±0.0034
11	0.0916±0.0038
12	0.0888±0.0041
13	0.0845±0.0044
14	0.0782±0.0044
15	0.0771±0.0053
16	0.0648±0.0050
17	0.0599±0.0050
18	0.0597±0.0052
19	0.0576±0.0055
20	0.0575±0.0060
21	0.0427±0.0063

The maximum correction to the absolute cross section owing to systematic errors in this experiment may be as much as 5%. To this should be added the systematic error introduced by the finite solid angle subtended by the detectors, which was calculated to be less than 0.75%; the absolute cross section reported here may be too low by this amount.

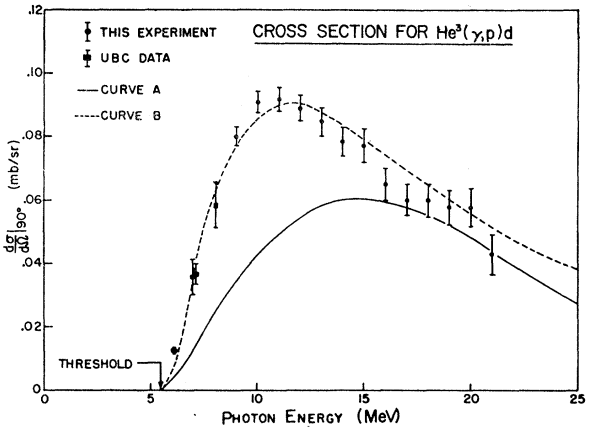

FIG. 12. Experimental and theoretical 90° differential cross sections for $He^3(\gamma,p)d$. Curve A results from the Gaussian ground-state wave function for He^3 of Verde (Ref. 1); curve B, from the modified exponential wave function of Gunn and Irving (Ref. 2), with $1/\mu=2.6$ F. The square points represent the data from recent experiments at the University of British Columbia (Ref. 20). No normalization has been performed.

Finally, as another check on the internal consistency of the experiment in addition to the satisfactory agreement of 0.5 V/cm and 1 V/cm data and of the data from the two pairs of counters, the 1 V/cm data were divided in half according to the dates when the experimental runs were taken; the results for the first half of the data were consistent in all ways with the results for the second half.

Information about the relative 3-body photodisintegration cross sections can be obtained from the $p\text{-}p$ events. The number of events in each 2-MeV bin of photon energy is divided by the corresponding number of photons in the bremsstrahlung spectrum and by the integrated beam flux, as before. The results are summarized in Table III, and the relative cross section for the two protons emitted back-to-back is shown in Fig. 13. For 3-body disintegrations where the two protons are emitted at right angles to each other and to the incident photon, the kinetic energy T_n of the neutron is equal to the sum of the kinetic energies of the protons, or

$$T_n=T_1+T_2=(k-\delta')/2\,, \tag{8}$$

where T_1, T_2, and δ' are the same as in Eq. (5) and again

TABLE III. Three-body cross section data ($\theta=180°$).

k(MeV)	$\frac{d^2\sigma}{d\Omega_1 d\Omega_2}$ (relative units)
9	0.0017±0.0005
11	0.0261±0.0044
13	0.0540±0.0066
15	0.0845±0.0096
17	0.0892±0.0099
19	0.0638±0.0087
21	0.0540±0.0092

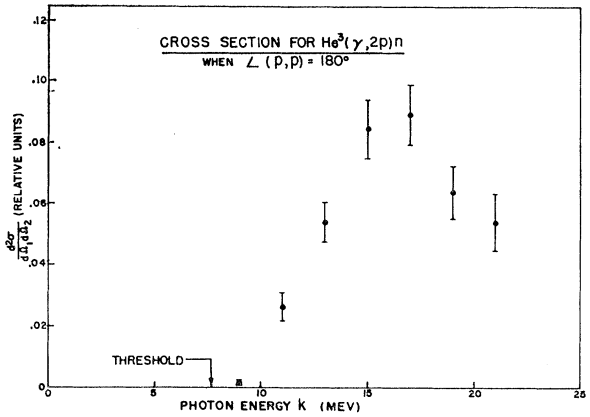

FIG. 13. Experimental double differential cross sections for $He^3(\gamma,2p)n$ when the two outgoing protons are emitted back-to-back.

the photon momentum is neglected. There were too few of these 90° events to obtain the energy dependence of the cross section (126 altogether), especially since the geometry allowed a large kinematical spread, but the total number (118) for $8 \leq k \leq 22$ MeV can be compared with the number of back-to-back (180°) p-p events, normalized to the same incident flux. The experimental ratio of the 180° p-p cross section to the 90° p-p cross section was found to be 6.50 with a statistical uncertainty of order 20%.

IV. DISCUSSION AND CONCLUSIONS

A. Two-Body Photodisintegration

Besides the early work of Cranberg,[6] four other experimental investigations of the photodisintegration of He^3 have been undertaken, and some preliminary results of these experiments are available. Schlüpmann *et al.*,[18] use electronic pulse-shape discrimination in an experiment otherwise similar to this one but over the range 14 to 29 MeV. Over this range, their 90° 2-body differential cross section falls smoothly from 0.10 to 0.03 mb/sr. Stewart and O'Connell[19] use a magnetic spectrometer to focus single protons and deuterons onto a semiconductor detector with a 40-MeV electron linac as a bremsstrahlung source. Their cross section reaches a peak of 0.09 mb/sr at 12 MeV and falls to 0.03 mb/sr at 30 MeV. The results of both these experiments agree, within the quoted errors, with those of the experiment reported here.

Gorbunov and Varfolomeev[20] used a cloud chamber filled with He^3 gas in the bremsstrahlung beam of a 170-MeV synchrotron. On the basis of about 150 events, they find a total cross section for the 2-body disintegration which has a maximum of 1.2 mb at $k=18$ MeV, and decreases to less than 0.1 mb between 60 and 90 MeV. They find, with low statistical accuracy, an angular distribution which approximates $\sin^2\theta$. Thus, their total cross sections can be multiplied by $3/8\pi$ to compare with 90° differential cross sections. Comparison of their results with the present experiment shows a strong discrepancy both in the magnitude and the shape of the cross section.

Warren *et al.*[21] used a cylindrical gridded ionization chamber filled with methane, argon, and He^3 as their detector, and used various nuclear reactions induced by 0.4 to 1.8 MeV protons from an electrostatic generator to produce monochromatic γ rays of several energies. Their results are shown in Fig. 12. Their results also agree to within 5% with the results of the measurement of the inverse cross section $p+d \rightarrow He^3+\gamma$, done by Griffiths *et al.*,[10,11,22] when related by detailed balance.

Several theoretical calculations have been made of the 2-body photodisintegration cross sections of 3-particle nuclei,[1-3] all based on ground-state wave functions which are totally symmetric in the space coordinates. Verde[1] has shown that the magnetic dipole transition into a final state which consists of a ^3S deuteron and a free nucleon is forbidden, which is in agreement with the observed low-capture cross section for thermal neutrons by deuterons, and also with the investigations of the $d(p,\gamma)He^3$ reactions discussed in Sec. I. Since all the evidence points to the electric dipole transition being dominant in the $He^3(\gamma,p)d$ reaction in the energy region under consideration, the theoretical total cross sections were multiplied by $3/8\pi$ to convert them into differential cross sections at 90°.

Curve A in Fig. 12 shows the cross section calculated by Verde[1] for a Gaussian ground-state wave function

$$\psi_{He} \propto \exp[-\mu^2 \sum_{i<j} r_{ij}^2], \tag{9}$$

where r_{ij} is the distance between the ith and jth nucleons in the nucleus, and μ is a size parameter found by equating the difference in binding energy of He^3 and H^3 (=0.76 MeV) to the Coulomb energy of He^3, which depends on the size of the nucleus. Verde used $1/\mu=5.5$ F. The energy dependence of the total cross section σ is

$$\sigma \propto (k-\delta)^{3/2} k \exp[-M(k-\delta)/3\mu^2], \tag{10}$$

where M is the nucleon mass, and units for which $\hbar=1$

[18] K. Schlüpmann *et al.* (private communication).

[19] J. R. Stewart and J. S. O'Connell, Yale Electron Accelerator Laboratory Internal Report, 1963 (unpublished); Postdeadline Paper, Meeting of the American Physical Society, Washington, D. C., April 1963 (unpublished), and J. S. O'Connell (private communication).

[20] A. N. Gorbunov and A. T. Varfolomeev, Phys. Letters 5, 149 (1963).

[21] J. B. Warren, K. L. Erdman, L. P. Robertson, D. Axen, and J. R. MacDonald, Bull. Am. Phys. Soc. 8, 124 (1963) and Phys. Rev. 132, 1691 (1963). Thanks are due to Dr. MacDonald for communicating his results prior to publication.

[22] The absolute cross sections published in Ref. 11 are in error; the re-evaluated data agree with the results in Fig. 12. J. R. MacDonald (private communication).

are used. Gunn and Irving[2] also have calculated σ with Gaussian wave functions for $1/\mu=4.2$ and 3.65 F. The results in all cases show that if μ is chosen to fit the maximum cross section, the position of the peak is too high in energy to agree with this experiment; and if it fits the energy of the peak, the corresponding cross section is much too large.

In addition, Gunn and Irving[2] calculated the cross section for a modified exponential ground-state wave function

$$\psi_{\mathrm{He}} \propto \exp[-\mu(\sum_{i<j} r_{ij}^2)^{1/2}]/(\sum_{i<j} r_{ij}^2)^{1/2}, \quad (11)$$

where μ is an arbitrary size parameter. The result is Curve B of Fig. 12, where the chosen value of the size parameter $1/\mu=2.6$ F gives a good fit to the data. A 5% change in $1/\mu$ spoils the fit noticeably. The analytical form of the cross section is given by

$$\sigma=32e^2\mu^4M^{-3}W_d^{-11/2}(k-\delta)^{3/2}k[F(\lambda)]^2, \quad (12)$$

where $W_d=2.23$ MeV is the binding energy of the deuteron, and

$$F(\lambda)=\frac{7\lambda-2}{\lambda^2(\lambda-1)^2}-\frac{15}{(\lambda-1)^3}+\frac{15}{(\lambda-1)^{7/2}}\cos^{-1}(\lambda^{-1/2}) \quad (13)$$

with

$$\lambda=\frac{1}{W_d}\left(k-\delta+\frac{3\mu^2}{2M}\right). \quad (14)$$

The wave function ψ_d for the deuteron in the final state was taken to be

$$\psi_d \propto s^{-1}\exp[-(MW_d)^{1/2}s], \quad (15)$$

where s is the relative coordinate of the two nucleons in the deuteron.

The mean-square nuclear radius of He^3 was calculated with the Gunn and Irving wave function

$$\langle r^2\rangle_{\mathrm{He}}=\frac{\int d^3r\,d^3s[\frac{1}{3}(\frac{3}{2}r^2+\frac{1}{2}s^2)]|\psi_{\mathrm{He}}|^2}{\int d^3r\,d^3s|\psi_{\mathrm{He}}|^2}=5/9\mu^2, \quad (16)$$

where r is the coordinate of one of the nucleons in the nucleus with respect to the center of mass of the nucleus, s is the relative coordinate of the other two, and the quantity in brackets is the average square of the distance from a nucleon to the center of mass. If $1/\mu=2.6$ F, then the root-mean-square nuclear radius $(\langle r^2\rangle_{\mathrm{He}})^{1/2}=1.94$ F. The mean-square charge radius $\langle r_{\mathrm{ch}}^2\rangle_{\mathrm{He}}$ is obtained approximately by adding the mean-square nuclear radius of He^3 to the mean-square charge radius of the proton

$$\langle r_{\mathrm{ch}}^2\rangle_{\mathrm{He}}=\langle r^2\rangle_{\mathrm{He}}+\langle r_{\mathrm{ch}}^2\rangle_p. \quad (17)$$

Using $(\langle r^2\rangle_p)^{1/2}=0.805$ F,[23] then $(\langle r_{\mathrm{ch}}^2\rangle_{\mathrm{He}})^{1/2}=2.1$ F in agreement with the recent electron-scattering measurements of Collard and Hofstadter.[24]

The wave function, Eq. (11), with the value $1/\mu=2.6$ F found in this experiment can be compared more directly with the Collard and Hofstadter[24] results by means of the entire form factor, which is calculated as a function of the momentum transfer q:

$$F_{\mathrm{He}}(q^2)=\int d^3r\exp(i\mathbf{q}\cdot\mathbf{r})\rho_{\mathrm{He}}(r), \quad (18)$$

where the nuclear matter distribution is

$$\rho_{\mathrm{He}}(r)=\int d^3s|\psi_{\mathrm{He}}|^2. \quad (19)$$

Using ψ_{He} from Eq. (11), we obtain (see Appendix A)

$$F_{\mathrm{He}}(q^2)=\frac{864}{(q/\mu)^2}\left[1-\frac{1+\frac{1}{12}(q/\mu)^2}{[1+(1/18)(q/\mu)^2]^{3/2}}\right]. \quad (20)$$

Values of F_{He} obtained from Eq. (20) were multiplied by the charge form factor of the proton[25,26]; this calculated charge form factor for He^3 agrees very well with the electron-scattering measurements at small q^2, and becomes larger than the measured one by about 20% only at values of q^2 approaching $5F^{-2}$ (Fig. 14).

B. Three-Body Photodisintegration

The results of Sec. III on the 3-body photodisintegration are limited not only by poor statistical accuracy but also by systematic errors resulting from the fact that the effective target volume for these events is limited by the brass walls of the target chamber and not by kinematics as for the 2-body events. Nevertheless, if rough estimates are made for the effective target volume and solid angles, some quantitative statements about the 3-body breakup can be made. The cross section for events in which the two protons go off at 180° to each other and 90° to the beam is given in Fig. 13. The "relative units" given there are an estimate of the absolute double differential cross section in mb/sr^2.

If the assumption is made that the cross section for 3-body breakup is proportional only to the volume available in phase space, with no variation of the matrix element with the angle between the outgoing protons, the ratio of events where the protons are emitted at 180° to each other to those where they are emitted at 90°

[23] L. N. Hand, D. G. Miller, and R. Wilson, Rev. Mod. Phys. **35**, 335 (1963).

[24] H. Collard and R. Hofstadter, Phys. Rev. **131**, 416 (1963).

[25] F_{ch} is defined by Eq. (A23) in D. R. Yennie, M. M. Levy, and D. G. Ravenhall, Rev. Mod. Phys. **29**, 144 (1957).

[26] Experimental values for the proton were taken from F. Bumiller, M. Croissiaux, E. Dally, and R. Hofstadter, Phys. Rev. **124**, 1623 (1961).

to each other would be 5.7 (see Appendix B). When the finite size of the crystals is taken into account, this figure is reduced to 5.3. The value of 6.5 ± 1.3 found in this experiment is therefore in acceptable agreement, and indicates no marked angular correlations between particles except those predicted by phase-space arguments.

Some statements about the relative magnitude of the 2- and 3-body disintegration processes can be made if the 3-body angular correlations are assumed to be purely statistical. When $dN/d\mu$ of Eq. (B8) is normalized to unity at $\mu=-1$ and integrated over all values of μ and ϕ, the result is 3.3. Therefore, the single differential cross section for a proton from 3-body breakup to be emitted at 90° to the beam is 3.3 times the double differential cross section for two protons to be emitted at 90° to the beam and 180° to each other, i.e., 3.3 times the values of Fig. 13. Since the values of Fig. 13 found in this experiment are about equal numerically to the 2-body cross sections of Fig. 12, and if the 2- and 3-body angular distributions are the same, then the 3-body differential cross section is about 3.3 times the 2-body cross section.

A reasonable estimate of the dipole sum given by Rustgi[27] is

$$\sigma_{\text{int}}=40[1+0.55(x+0.5y)]=58 \text{ MeV-mb}, \quad (21)$$

where $(x+0.5y)$ has been taken as 0.8.[28] Since integration of the 2-body cross section to 40 MeV, using the wave function of Eq. (11) with $1/\mu=2.6$ F, gives only 13 MeV-mb, it is clear that the 2-body cross section should make up about 25% of the total. This is in accord with the calculations of Gunn and Irving and with the fragmentary evidence on 3-body disintegration presented here.

ACKNOWLEDGMENTS

The cooperation of the betatron engineers and staff is gratefully acknowledged. Eugene W. Beier, John R. O'Fallon, and Nancy M. O'Fallon assisted in taking and processing the data. Professor G. Ascoli, Professor J. D. Jackson, and Professor D. G. Ravenhall made several valuable suggestions. Dr. G. dePasquali aided in the preparation of the crystals.

APPENDIX A: CALCULATION OF THE He^3 NUCLEAR FORM FACTOR

The nuclear matter distribution is, from Eq. (19),

$$\rho_{\text{He}}(r)\propto\int d^3s\frac{\exp[-2\mu(\frac{3}{2}s^2+\frac{9}{2}r^2)^{1/2}]}{\frac{3}{2}s^2+\frac{9}{2}r^2}. \quad (A1)$$

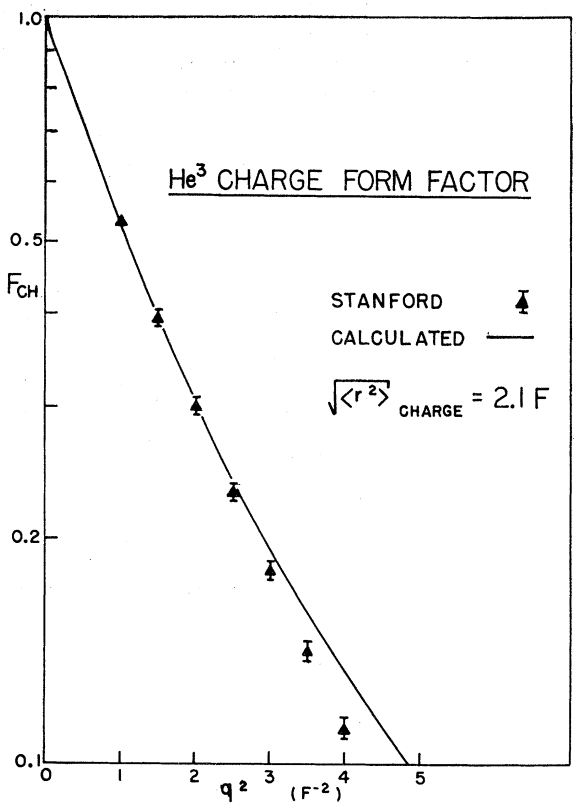

FIG. 14. He^3 charge form factor from (i) Gunn and Irving wave function with $1/\mu=2.6$ F, and (ii) electron scattering measurements.

Therefore, from Eq. (18),

$$F_{\text{He}}(q^2)\propto\int_0^\infty s^2ds\int_0^\infty r^2dr\frac{\sin qr}{qr}\times\frac{\exp[-2\mu(\frac{3}{2}s^2+\frac{9}{2}r^2)^{1/2}]}{\frac{3}{2}s^2+\frac{9}{2}r^2}. \quad (A2)$$

Letting $x=6^{1/2}s\mu$, $y=3\sqrt{2}r\mu$, $\alpha=(\sqrt{2}/6)(q/\mu)$, we get

$$F_{\text{He}}(q^2)\propto\int_0^\infty x^2dx\int_0^\infty ydy\sin\alpha y\frac{\exp[-(x^2+y^2)^{1/2}]}{x^2+y^2}. \quad (A3)$$

Letting $x=R\sin\theta$, $y=R\cos\theta$, we get

$$F_{\text{He}}(q^2)\propto\int_0^{\pi/2}d\theta\sin^2\theta\cos\theta\int_0^\infty R^2dR\times\sin(\alpha R\cos\theta)e^{-R}, \quad (A4)$$

whence

$$F_{\text{He}}(q^2)\propto\int_0^{\pi/2}d\theta\sin^2\theta\cos^2\theta\frac{1+A\cos^2\theta}{(1+B\cos^2\theta)^3}, \quad (A5)$$

[27] M. L. Rustgi, Phys. Rev. **106**, 1256 (1957).
[28] L. Rosenfeld, *Nuclear Forces* (North-Holland Publishing Company, Amsterdam, 1948), p. 234.

where $A=-\alpha^2/3$ and $B=\alpha^2$. So

$$F_{He}(q^2)\propto\frac{d^2}{dB^2}\int_0^{\pi/2}d\theta\frac{\sin^2\theta}{\cos^2\theta}\frac{1+A\cos^2\theta}{1+B\cos^2\theta} \quad \text{(A6)}$$

and the integral in Eq. (A6) becomes

$$\int\tan^2\theta d\theta+(A-B)\int\frac{\sin^2\theta d\theta}{1+B\cos^2\theta}$$

$$=\tan\theta-\frac{A}{B}\theta+\frac{A-B}{B}(1+B)^{1/2}$$

$$\times\tan^{-1}[(1+B)^{-1/2}\tan\theta], \quad \text{(A7)}$$

whence

$$F_{He}(q^2)\propto-\frac{\pi A}{B^3}+\frac{\pi}{2}\left[\frac{B-A}{4B}(1+B)^{-3/2}\right.$$

$$\left.-\frac{A}{B^2}(1+B)^{-1/2}+\frac{2A}{B^3}(1+B)^{1/2}\right], \quad \text{(A8)}$$

or

$$F_{He}(q^2)\propto 1-\frac{1+\frac{3}{2}\alpha^2}{(1+\alpha^2)^{3/2}}. \quad \text{(A9)}$$

Normalizing to $F_{He}=1$ at zero-momentum transfer results in Eq. (20).

APPENDIX B: THREE-BODY PHASE SPACE

We have, from Eq. (5),

$$T_1+T_2+(T_1T_2)^{1/2}\mu=Q/2, \quad \text{(B1)}$$

where $\mu=\cos\theta$ and $Q=k-\delta'$. Setting $x=(T_1+T_2)/Q$, $y=(T_1-T_2)/Q$ yields

$$y^2=x^2-[(1-2x)/\mu]^2. \quad \text{(B2)}$$

The volume in phase space for this reaction is proportional to dT_1dT_2, and hence to $dxdy$. We choose to solve for the cross-section differential in solid angle $d\Omega=d\phi d\mu$, which is found by integrating over T_1 (or x), since for a given μ, T_2 (or y) is fixed by T_1 (or x):

$$\frac{dN}{d\mu}\propto\int\frac{\partial y}{\partial\mu}dx. \quad \text{(B3)}$$

The limits on x are

$$\begin{aligned}&\tfrac{1}{2}\le x\le\frac{1}{2+\mu}=\frac{1}{2-|\mu|} && \text{for } \mu<0\\ &\frac{1}{2+\mu}\le x\le\tfrac{1}{2} && \text{for } \mu>0\end{aligned}. \quad \text{(B4)}$$

From Eq. (B2),

$$\frac{dy}{d\mu}=[(1-2x)/\mu]^2$$

$$\times\left[(4-\mu^2)\left(x-\frac{1}{2+\mu}\right)\left(\frac{1}{2-\mu}-x\right)\right]^{-1/2}. \quad \text{(B5)}$$

Let

$$x=(2-\mu\sin\xi)/(4-\mu^2). \quad \text{(B6)}$$

Then

$$\begin{aligned}\frac{dN}{d\mu}&\propto(4-\mu^2)^{-5/2}\int_{\sin^{-1}(\mu/2)}^{\pi/2}(\mu-2\sin\xi)^2d\xi && \text{for } \mu>0\\ &\propto(4-\mu^2)^{-5/2}\int_{-\sin^{-1}(|\mu|/2)}^{\pi/2}(|\mu|+2\sin\xi)^2d\xi && \text{for } \mu<0.\end{aligned} \quad \text{(B7)}$$

The integrals are done easily, yielding, in both cases,

$$\frac{dN}{d\mu}\propto(4-\mu^2)^{-5/2}\{(2+\mu^2)[(\pi/2)-\sin^{-1}(\mu/2)]$$

$$-[3\mu(4-\mu^2)^{1/2}/2]\}. \quad \text{(B8)}$$

This expression was integrated over the solid angle subtended by the counters for the cases where the two protons are emitted (a) back-to-back, and (b) at right angles to each other. In case (a), circular detectors of area equal to the square ones were used to approximate the real case. Here $(\Delta\phi)_a=2\pi$, and $\Delta\theta$ is given by

$$(\Delta\theta)_a=\tan^{-1}(2.83/5\pi^{1/2})=17.7^\circ. \quad \text{(B9)}$$

In case (b),

$$(\Delta\theta)_b=2\tan^{-1}(1.41/5)=31.6^\circ, \quad \text{(B10)}$$

and $(\Delta\phi)_b\cong(\Delta\theta)_b$. The integrations over θ were done graphically, resulting in $N_a/N_b=0.47$, where $N=\int(dN/d\mu)d\mu$, and the limits of integration determine the appropriate case. Hence,

$$\frac{N_a(\Delta\phi)_a}{N_b(\Delta\phi)_b}=(0.47)\frac{360^\circ}{31.6^\circ}=5.3. \quad \text{(B11)}$$

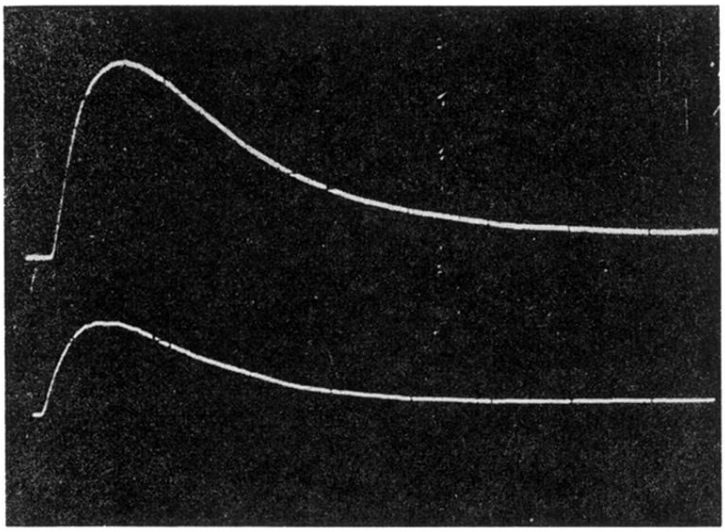

FIG. 4. Oscilloscope photograph of a typical $He^3(\gamma,p)d$ event.